



HAL
open science

On the numerical methods for tracking a European eel motion in a closed-conduit system

Islam Abdelghafar, Jonathan D Bolland, Dominique Thévenin, Philip A Rubini, Rosalind M Wright, Stefan Hoerner

► **To cite this version:**

Islam Abdelghafar, Jonathan D Bolland, Dominique Thévenin, Philip A Rubini, Rosalind M Wright, et al.. On the numerical methods for tracking a European eel motion in a closed-conduit system. IAHR 10th International Symposium on Hydraulic Structures, ETH Zurich, Jun 2024, Zurich, Switzerland. 10.3929/ethz-b-000676016 . hal-04642586

HAL Id: hal-04642586

<https://hal.science/hal-04642586>

Submitted on 9 Jul 2024

HAL is a multi-disciplinary open access archive for the deposit and dissemination of scientific research documents, whether they are published or not. The documents may come from teaching and research institutions in France or abroad, or from public or private research centers.

L'archive ouverte pluridisciplinaire **HAL**, est destinée au dépôt et à la diffusion de documents scientifiques de niveau recherche, publiés ou non, émanant des établissements d'enseignement et de recherche français ou étrangers, des laboratoires publics ou privés.



Distributed under a Creative Commons Attribution 4.0 International License

On the numerical methods for tracking a European eel motion in a closed-conduit system

Conference Paper**Author(s):**

Abdelghafar, Islam; Bolland, Jonathan D.; Thévenin, Dominique; Rubini, Philip A.; Wright, Rosalind M.; Hoerner, Stefan

Publication date:

2024

Permanent link:

<https://doi.org/10.3929/ethz-b-000676016>

Rights / license:

[Creative Commons Attribution 4.0 International](#)

On the numerical methods for tracking a European eel motion in a closed-conduit system

Islam Abdelghafar^{1,2,3}, Jonathan D. Bolland¹, Dominique Thévenin³, Philip A. Rubini², Rosalind M. Wright⁴ & Stefan Hoerner^{3,5}

¹Hull International Fisheries Institute, School of Natural Sciences, University of Hull, HU6 7RX, UK

²School of Engineering, University of Hull, HU6 7RX, UK

³Laboratory of Fluid Dynamics and Technical Flows, Otto von Guericke University Magdeburg, 39106, Germany

⁴Environment Agency, Rivers House, Threshelfords Business Park, Inworth Road, Feering CO5 9SE, UK

⁵LEGI, Université Grenoble Alpes, CNRS, Grenoble INP, 38000, France

E-mails: i.abdelghafar-2022@hull.ac.uk; islam.abdelghafar@ovgu.de

Abstract: The European eel (*Anguilla anguilla*) is distributed from the North Cape in Norway, southwards along the coast of Scandinavia and the Baltic states throughout Atlantic Europe and all the coasts of the Mediterranean including North and West African Coast. It can be found in a wide variety of freshwater and estuarine habitats. In the past three decades, a dramatic decline in the number of eels reaching European river systems has been recorded. European eel is listed as "critically endangered" under the IUCN red list of the threatened species. Hydraulic structures across rivers (e.g. low-head weirs) and other in-river anthropogenic barriers (e.g., pumping stations, hydropower facilities) impede downstream migration of European eels. The identification of hazardous regions in technical facilities and their assessment in an early design phase is necessary to achieve safe migration. Computational fluid dynamics (CFD) provide a great variety of approaches to simulate fluid flows and allow for the implementation of fish and eel surrogate models without the need of doing live fish tests. Various numerical approaches with varying modelling complexities for tracking European eel motion including streamlines, particle-based methods, and Dynamic fluid/body Interaction (DFBI) were investigated in the present study. A closed-conduit component, typically, a flanged eccentric reducer is considered as a test case to demonstrate the different numerical approaches. One of the early attempts is to treat a fish trajectory as a streamline and all relevant flow quantities (e.g., velocity, pressure, shear stress) could be derived along this path. A more recent tracking method for fish or eel motion is to include a Lagrangian approach, in which the eel is approximated as a super-ellipsoid particle, composite particles, or a Flexible Fiber composed of bonded segments with the aid of the Discrete Element Method (DEM). Finally, a boundary resolved approach, Dynamic Fluid-Body Interaction (DFBI), can be used efficiently to track the eel motion by solving the equations of motion with 6 degrees of freedom (6-DOF) coupled with the fluid flow. The DFBI motion can be combined either with overset Chimera or overlapping meshes to track rigid bodies or with an additional body morphing function which allows for the tracking of flexible bodies. DFBI combined with overset meshes is a highly accurate approach and provides very precise insights in the fluid-body interactions of eels in a surrounding fluid due to the resolved boundaries. However, it has drawbacks in terms of computational cost and complexity of mesh construction. A qualitative comparison of the proposed numerical approaches for tracking eel motion through a closed-conduit is addressed in terms of accuracy, computational cost, and contact modelling.

Keywords: Closed-conduit, pipe fittings, eel motion, CFD-DEM, overset 6-DOF.

1. Introduction

The European eel (*Anguilla anguilla*) is classified as critically endangered under the IUCN red list of the threatened species (Pike et al., 2020). Mature adult eels (known as silver eels) migrate down rivers and travel thousands of kilometers to spawn in the Sargasso Sea in the North Atlantic Ocean (Wright et al., 2022). The leptocephalus return across the North Atlantic Ocean to Europe and North Africa to migrate up rivers as glass eels and elvers (Piper and Wright, 2017). Its complex life cycle makes this species vulnerable to man-made barriers and hydraulic structures that hinder its upstream immigration and downstream spawning migration, such as weirs, low- to high-head dams, sluices, spillways and closed-conduit systems for pumping water or hydropower generation (Belletti et al., 2020, Watson et al. 2018). Fishways, sluices and bypass facilities could be solutions to remediate the migration of vulnerable species like European eels, protect biodiversity and maintain healthy eel populations (Carter et al., 2023). Generally, fish and eels go through two main categories of hydraulic structures, open-channel flow, and closed-conduit fishways and could be blocked by barriers on rivers (Cox et al., 2023). Fish and eels can migrate upstream or downstream through fishways, spillways or be entrained into hydraulic turbines and pumps. This paper focus only on closed-conduit components to assess the efficiency of various numerical approaches in tracking motion of eel-like objects through a contraction. It is common to find pipes of different diameters in any piping system; reducers are used to transition from a larger pipe to a smaller pipe, while expanders are used to transition from a smaller pipe

to a larger pipe. Fish and eels experience sudden changes through contractions and expansions which could cause injuries or mortality (Cox et al., 2023).

In recent years, there has been a steadily increasing interest in hydraulic structures that provide safe passage for the migrating fish, i.e., minimising the risk of fish injury and mortality. This requires reliable methods that empower hydraulic engineers and planners to design efficient hydraulic structures without harming fish and eels. Numerical methods, particularly Computational fluid dynamics (CFD) have been proven to be a valuable, reliable tool to enhance our understanding of flows across hydraulic structures and to quantify the sources of injury or mortality to fish and eels under some assumptions. Early approaches involved the simple assumption that a fish or an eel act as a flow streamline and all relevant quantities including velocity, pressure and shear stress were derived along this pathway (Garrison et al., 2002; Elena-Maria & Holger, 2020; Richmond et al., 2014). Streamlines are the most common geometric technique to represent fish paths, where a massless point seed at pre-defined release position is advected through the main flow, assuming that the seed velocity is equal to the flow velocity (Richmond & Romero-Gómez, 2014). The resulting pathway represents a case in which fish are passively carried along with the flow. Accordingly, using flow streamlines can be misleading since it ignores fish inertia (streamlines neither account for the mass nor the body length of a fish), own fish movement, and other body or surface forces that act on the fish (Koukouvinis and Anagnostopoulos, 2023).

Lagrangian approaches have since been used in fish tracking studies, in which the fish is approximated as a particle with a mass (sphere, cylinder, super-ellipse) or composite particles with the aid of Discrete Element Method (DEM) (Richmond & Romero-Gómez, 2014; Powalla et al., 2022). Compared to streamlines, a physical realism is added to the Lagrangian particles which results in increased computational cost. Unlike massless point seeds, Lagrangian particles are not simply passively advected through the domain but instead, the motion is determined by the fluid forces acting on the particle such as drag, pressure gradient, virtual mass effects and gravity. The Flexible Fiber model can also do the same function by connecting several identical DEM cylinders bonded end to end and these bonds can do axial extension and compression and bending deformations (Siemens Digital Industries Software 2023). More accurate and complex methods such as overset six-degree of freedom (6-DOF) and Immersed Boundary Method (IBM, see Huang et al., 2022) have recently been adopted to track fish motion. However, such methods commonly result in extremely high computational cost and not suitable for neither practical applications nor statistical analyses. Recently, an uncoupled 6-DOF tracking approach has been suggested by Koukouvinis and Anagnostopoulos (2023) using an approximated pressure field about the tracked object. The advantage of such an approach is that the pressure field can be obtained from a steady-state flow simulation. Contact modeling in-between the tracked object and the walls has been considered in the uncoupled 6-DOF approach. However, the current work only focuses on the computationally expensive coupled overset 6-DOF approach to predict rigid eel motion in a closed-conduit fishway and compare it to other fast numerical approaches based on CFD-DEM which apply empirical laws for fluid interactions. Most of the current research focused on either experimental work or low-fidelity numerical methods that ignore important physics related to the fish motion through different hydraulic structures and a general lack of base studies which validate more advanced numerical methods has to be stated. In this work, a flanged eccentric reducer (ASME/ANSI B16.1 – Class 125), as a simple closed-conduit component, was considered to demonstrate and compare four numerical methods in terms of accuracy, computational cost, and modeling of the contact in-between traveling objects and walls. Based upon this comparison, new insights into the features and costs of various numerical approaches with varying modelling complexities ranging from flow streamlines (the simplest approach) to particle-based methods ending with the boundary-resolved 6-DOF method (the most complex approach) for fish/eel tracking were presented.

2. Methodology

In this study, all numerical simulations were carried out using the commercial CFD software Star-CCM+ to model the flow through a closed-conduit component. The particles are described in a Lagrangian framework, which means that each path of an injected particle is tracked when traveling through the domain. The continuous phase is described in an Eulerian framework and the combination of both leads to an Eulerian-Lagrangian multiphase flow model. The deployed Eulerian-Lagrangian multiphase model calculates the trajectory of each particle and the momentum equations for the fluid flow – taking all interactions between the dispersed phase (particles) and the continuous phase (water) into account. Different coupling levels are possible, in which only flow to particle information transfer is considered (one-way-coupling), or additionally the feedback of the particle onto the flow (two-way-coupling). Choosing the DEM model as a Lagrangian representation of the particle adds two more coupling levels, when considering particle-particle and/or particle-wall interaction. For this study, the particle-wall

interactions are more interesting because they correspond to eel-like objects (i.e., particle) – piping system (i.e., wall) interactions. The DEM model enables the recording of contact forces for collisions, which can be used for prediction models regarding eel mortality and injury risk. Overset meshing is a meshing technique which allows for a relatively convenient handling of complex motions and deformations (Sharma et al., 2020). It requires a background mesh, and one or more component meshes which overlap with the background mesh to deal with moving and deformed bodies. The connectivity between the background mesh and the component meshes is performed through interpolation techniques for the overlapping cells. Generally, it is well-established, accurate and reliable technique to handle 6-DOF moving bodies. However, it has some drawbacks: (1) very computationally expensive, (2) special requirements on mesh sizing for the overlapping cells, and (3) sensitivity of schemes for cell-cutting and grid priorities. For the CFD-DEM approach, three Lagrangian particle types are compared, namely, 1) super-ellipsoid particles, 2) composite particles which consist of 20 spherical sub-particles arranged together to represent the eel-like object, and 3) flexible fibers which use a number of identical segments (typically, 110 segments to resemble the number of vertebrae in the real European eel (Boetius, 1980) bonded end to end (see, Figure 1(a)-(c)). All the bonds of the flexible fiber can perform axial extension and compression and bending deformations. Each bond is controlled by normal stiffness and bending stiffness of two springs. For all CFD-DEM particles emulating the eel, drag models using Schiller-Naumann correlation, pressure gradient, and virtual mass are activated. Taking the advantage that overset 6-DOF methods can handle the complexity of real shapes including all geometrical features of objects, a real European eel geometry is also used in the present study (see Figure 1(d)). The real geometry of the European eel is created from a Computed Tomography (CT) scanned STL file provided by collaboration partners from Centre for Environmental Intelligence and Sensing, Tallinn University of Technology (TalTech). It has dimensions $37.73 \times 2.16 \times 3.47$ cm (length \times width \times height), mass of 81 g to maintain neutral buoyancy in water, and principal moments of inertia defined as $I_1 = 38.74$ g \cdot cm 2 , $I_2 = 5360.5$ g \cdot cm 2 , $I_3 = 5347.02$ g \cdot cm 2 (all off-diagonal moment of inertia components are set to zero). Based on the understanding of kinematics of fish and eels, it is found that rolling and pitching motions can be ignored for moving in 3D space (Xue et al. 2023). In the current numerical setup, the rigid eel has four-degrees of freedom; representing three translation motions in X, Y, and Z and one rotational motion around Y to achieve yawing motion. All the external forces including contact and fluid forces (drag, pressure and shear forces) are considered except for the gravitational force as the swim bladders in fishes and eels make them neutrally buoyant. It should be mentioned that all objects have the same length (37.73 cm) to allow for a fair comparison between the four different tracking approaches. For all numerical simulations, the tested flow velocity at the pipe inlet (V_{inlet}) is 390 cm \cdot s $^{-1}$ resulting in average flow rate ($Q = 191.44$ L \cdot s $^{-1}$) and average Reynolds number ($Re = 9.71 \times 10^5$) for water at ambient conditions.

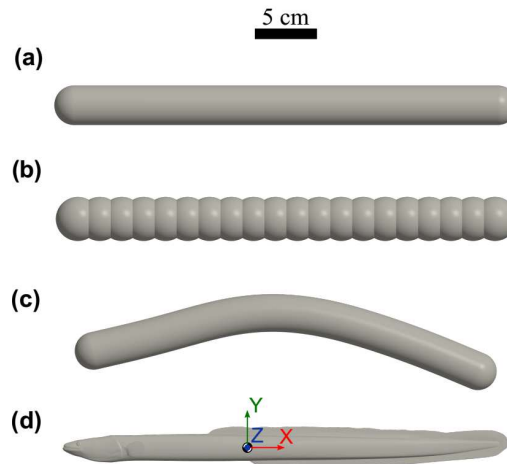


Figure 1. Representation of eel-like objects used for different tracking approaches. (a) CFD-DEM super-ellipsoid particle, (b) CFD-DEM composite particle, (c) CFD-DEM flexible fiber, compared to (d) Overset 6-DOF of a real, rigid eel.

2.1 Computational domain

During this study, a flanged eccentric reducer in a closed-conduit fishway (Figure 2) was considered to demonstrate different numerical methods used for tracking a European eel motion and quantify the flow conditions they experience. There are different forms of reducers, including concentric, eccentric, square and tapered. Here, a flanged eccentric reducer (ASME/ANSI B16.1 – Class 125) with an inlet diameter (D) of 25 cm and an outlet

diameter (d) of 15 cm was chosen to introduce both flow deflection and acceleration, and a rapid pressure drop across the pipe contraction.



Figure 2. Assembly for the considered flanged eccentric reducer (ASME/ANSI B16.1 – Class 125).

As an essential step for the CFD simulation, the geometry for a flanged eccentric reducer, representing contractions in closed-conduit fishways was created. The reducer has a length $l = 1D$ to connect a 25 cm pipe in diameter to a 15 cm. The entry and delivery pipes connected to the reducer are made of sufficient length to avoid secondary flow effects from contraction on the eel-like object transport. It is important for the entrance length to be sufficiently long to allow the flow to fully develop over the entrance to the closed-conduit component. Accordingly, the pipe sections are set to $7D$ for the entry pipe and $5D$ for the delivery pipe which is found to be sufficiently long to prevent any abrupt termination of the flow as shown in Figure 3. The inlet was set to a velocity inlet condition, where a uniform velocity profile was assumed for all faces on the boundary. For the outlet, a pressure outlet condition was defined, with a static pressure of 0 Pa relative to the operating pressure which is set to atmospheric pressure (101,325 Pa) in this simulation. The pipe walls were modeled as no-slip walls, and the roughness of the closed-conduit components is assumed to be like the roughness of the connecting pipes.

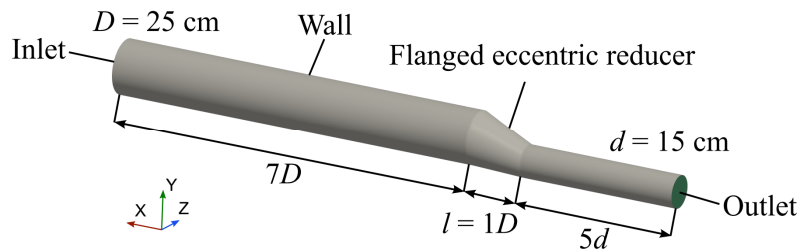


Figure 3. Computational domain showing the main dimensions and boundary conditions.

2.2 Computational mesh

A sample of the computational mesh for reducer is shown in Figure 4. The computational mesh in both configurations uses hexahedral trimmed cells with refinement towards the pipe walls. Five prism layers with stretching of 1.5 are adopted at the pipe walls to capture the near-wall gradients adequately, ensuring a maximum y^+ at inlet flow velocity of $390 \text{ cm}\cdot\text{s}^{-1}$ of around 102. The total number of cells for the reducer is about 0.678 million cells. Special setup is usually required for the overset 6-DOF approach to accommodate for the overset region that is embedded in the background region. The rigid eel was introduced into the computational domain as a component mesh, enclosed within a cylinder discretized with a lower prioritized cell size. All the relevant 6-DOF properties of the overset region containing the rigid eel (e.g., mass, principal moments of inertia) are defined. The background region representing the closed-conduit component (eccentric reducer) was discretized with a higher prioritized cell

size. The distance weighted interpolation option in Star-CCM+ was chosen to set the overset interface between a lower prioritized region (cylinder containing the rigid eel) and a higher prioritized region (closed-conduit). Furthermore, the Adaptive Mesh Refinement (AMR) technique was applied to the overset interface to match the cell size of the background region to the cell size of the overset region. It helps to ensure successful interpolation at the overset interface in each time-step without the need to increase number of cells of the background region.

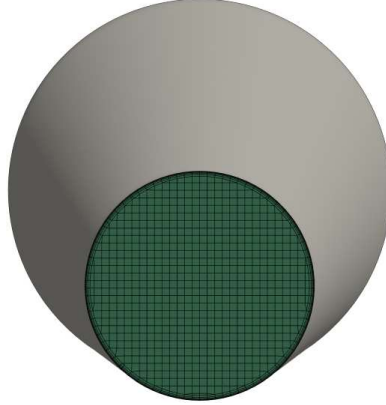


Figure 4. A sample of hexahedral mesh generated by the trimmed cell mesher at the outlet boundary.

2.3. Solver settings

The calculations were based on incompressible Unsteady Reynolds-Averaged Navier-Stokes (URANS) equations. To allow the closure of the time-averaged Navier-Stokes equations, the Reynolds stresses are estimated by employing a turbulence model. The high-Reynolds turbulence model SST $k - \omega$ was chosen due to its accuracy and reliability for wall-bounded flows (Rezaeiha et al., 2019). The pressure-velocity coupling is carried out using the segregated SIMPLE solver. The Venkatakrisnan limiter method is used to compute gradients (Siemens Digital Industries Software, 2023). The adaptive y^+ wall treatment model was enabled to accommodate all distinguished viscous regions within the boundary layer close to the wall. The spatial discretization was carried out using hexahedral trimmed cells alongside a mesh refinement in the vicinity of the pipe walls. The prism layer mesher was also enabled to accurately capture the high gradients that occur close to the walls. The Lagrangian multiphase model was used to describe the dispersed phase, in addition to the phase interaction models for DEM particles emulating the European eel properties and its behavior during contact with the pipe walls. For the CFD-DEM simulations in this study, the material properties of standard solid rubber (Arlon Thermabond 99180010) are used for all the different particle types to add some flexibility to the assigned particles. The density of the particles was set to be the density of water ($\rho = 0.998 \text{ g}\cdot\text{cm}^{-3}$), allowing the particles to act as a neutrally-buoyant object. When it comes to the 6-DOF approach, the Dynamic Fluid-Body Interaction (DFBI) combined with the overset mesh technique is required to simulate the motion of the rigid eel through the piping system. In the solver framework, the DFBI rotation and translation motion drives the 6-DOF overset region that contains the rigid eel body. The convergence of the numerical solution is judged by two parameters which are (1) maximum inner iterations in each time-step and (2) maximum physical time. It was found that 35 iterations per time step is enough to reduce the scaled residuals of the continuity and X-, Y- and Z-momentum equations by two orders of magnitude. The through-flow time (T_f) is defined based on the average flow velocity in the upstream and downstream pipes. Generally, the center of mass of the eel-like object is tracked over time using CFD-DEM and overset 6-DOF approaches, resulted in the object trajectory. All the tracked eel-like objects in this study were released from the center of the pipe near the inlet boundary at $x = 3D$ and at release time $t_s = 8.90 \text{ s}$ ($\approx 15T_f$) with initial traveling speed equal to zero. To reach a quasi-steady state and converged solution for the flow around the eel-like objects, the simulation was allowed to run for a physical time equal to 15 times the corresponding through-flow time. All the relevant solver settings for the current numerical setup are listed in Table 1.

Table 1. Overview of solver settings.

Solver physics	Three dimensional, Implicit unsteady, Incompressible, Turbulent, Segregated flow
Pressure-velocity coupling algorithm	SIMPLE
Gradients model	Venkatakrisnan limiter

Turbulence model	(Menter) SST $k - \omega$
Wall treatment model	Adaptive y^+ wall treatment
Mesh motion model (only for overset 6-DOF approach)	DFBI rotation and translation
Eulerian-Lagrangian multiphase model (only for CFD-DEM approach)	Discrete Element Method (DEM)
Overset mesh (only for overset 6-DOF approach)	
Background region	Piping system (base cell size = 1 cm)
Overset region	Rigid eel (base cell size = 0.5 cm)
Interpolation option	Distance weighted
Spatial discretization	
Mesher	Trimmed cell mesher, prism layer mesher
Temporal discretization	
Accuracy level	1 st -order
Time-step	$1 \cdot 10^{-3}$ s
Stopping criteria	
Maximum inner iterations in each time-step	35 iterations
Maximum physical time	$15T_f$ s (T_f = Through-flow time)

3. Results

It is known from the continuity equation that the reduction in cross-section area results in an increase in flow velocity. According to Bernoulli's equation, static pressure before the eccentric reducer is proportionately higher in comparison to the static pressure in the outlet pipe. It was found that the flow accelerated from $390 \text{ cm}\cdot\text{s}^{-1}$ to a maximum flow velocity of $1500 \text{ cm}\cdot\text{s}^{-1}$ at the exit of an eccentric reducer of length $l = 1D$, as shown in Figure 5. Referring to the velocity contours (see Figure 5) at entry and exit of eccentric reducer cross-section, a low-velocity zone close to the extrados at location 1 ($x = 7D$) is switched to a high-velocity zone at location 2 ($x = 8D$).

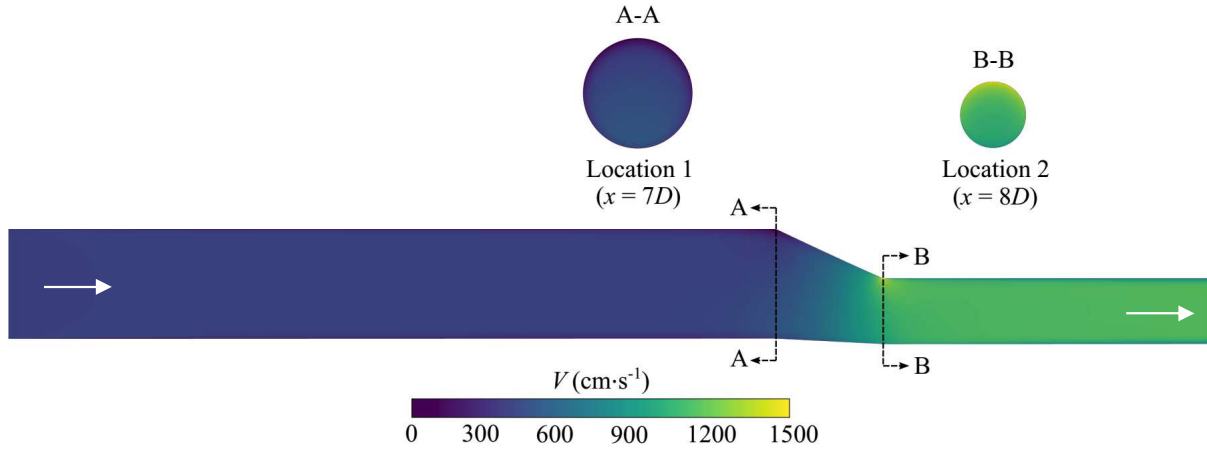


Figure 5. Contour of velocity magnitude V of an eccentric reducer at inlet flow velocity $V_{\text{inlet}} = 390 \text{ cm}\cdot\text{s}^{-1}$.

Figure 6 shows the trajectories corresponding to four CFD methods at different instants in time corresponding to four spatial positions; release location, entrance into the eccentric reducer, passing through the eccentric reducer, and pipe outlet where atmospheric pressure is defined. The objects generally accelerated through the eccentric reducer then the rate of change of velocity became constant after leaving the eccentric reducer heading toward the outlet. The comparison of acceleration, yaw angle (the third Euler angle), pressure and contact force data for the four tracking numerical approaches at the same inlet flow velocity showed remarkable disparity (Figure 7(a)-(d)). At the entrance of the eccentric reducer, a sharp acceleration was observed with a maximum acceleration greater than $500 L\cdot\text{s}^{-2}$ (where L is the eel-like object length) in case of both super-ellipsoid particle and composite particles whereas the predicted maximum acceleration is less than $500 L\cdot\text{s}^{-2}$ for flexible fiber and rigid eel methods. It can be noticed in Figure 7(a) and 7(b) (middle panel) that there was an acceleration spike of negative value once the object left the eccentric reducer. This spike of negative acceleration occurred due to the contact between the object (here, super-ellipsoid particle and composite particles) and the pipe walls which is not the case in Figure 7(c) and (d) in which no contact is detected. The yaw angle of the traveling objects was constant and showed a slight change near the exit of

the delivery pipe. The gauge pressure became stable (≈ 56.51 kPa) along the distance between the release location and the entrance of the eccentric reducer as shown in Figure 7 (lower panel). A sharp dip in pressure was recorded as the eel-like object traveled through the eccentric reducer due to contraction. As the eel-like object left the eccentric reducer, it traveled through the delivery pipe and the gauge pressure was atmospheric (0 kPa). The spike in the contact force diagram (lower panel) indicates a collision of the object with the pipe wall as seen in Figure 7(a) and (b) while the contact force is zero when flexible fiber and rigid eel are employed (Figure 7(c) and (d)). In the same context, similar observations have been reported in (Cox et al. 2022) using life fish experiments on juvenile silver perch and compared it to the data obtained from a neutrally buoyant sensor travelling through a tube fishway. For the tested flow rate ($Q = 8.4 \text{ L}\cdot\text{s}^{-1}$), the sensor measured an acceleration of 16G and a ratio pressure change (RPC) of 1.25 when it passed through a tapered contraction which has a contraction ratio equal to 3 and exit pipe diameter of 5 cm (Cox et al. 2022).

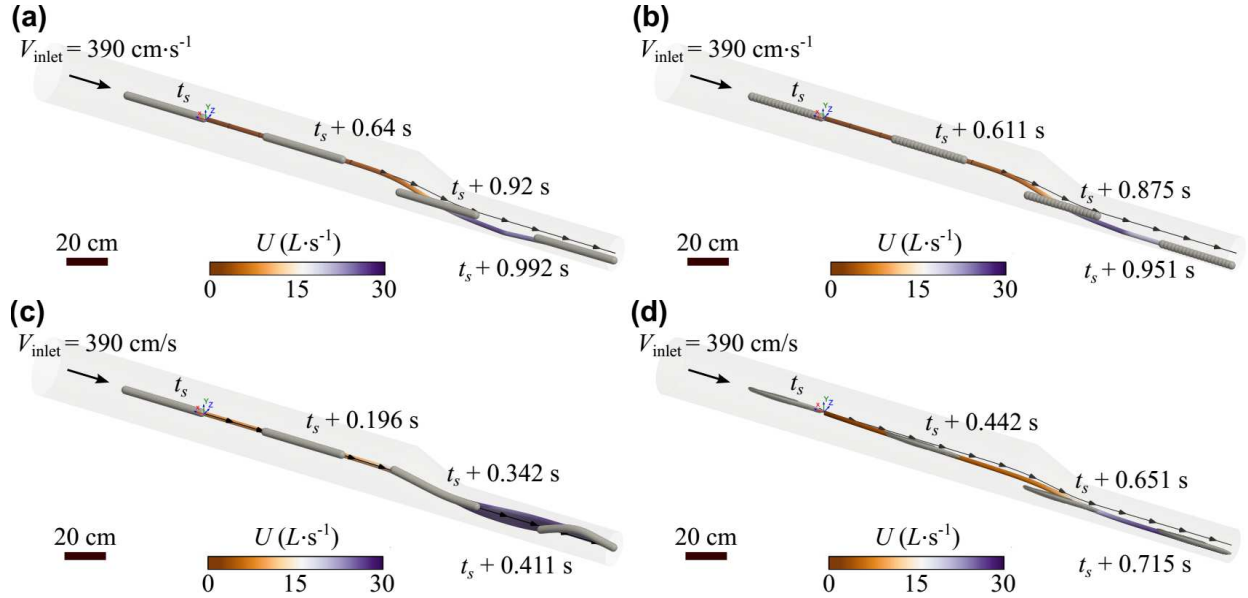
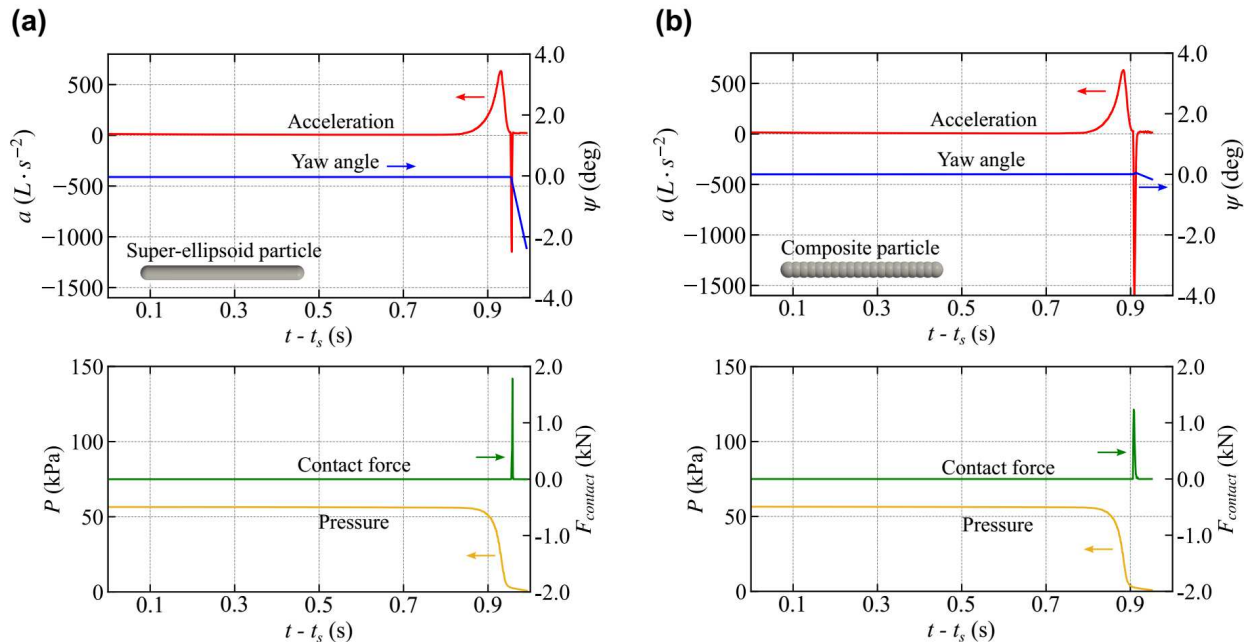


Figure 6. Object trajectories colored by traveling speed magnitude U (see, colormap) with overlaid object shapes at several instants in time $t - t_s$ through an eccentric reducer for an inlet flow velocity $V_{\text{inlet}} = 390 \text{ cm}\cdot\text{s}^{-1}$. The object trajectory is compared to the corresponding streamline using massless point seed (black line with markers at geometric distance of 15 cm). (a) CFDEM super-ellipsoid particle, (b) CFDEM composite particle, (c) CFDEM flexible fiber, (d) Overset 6-DOF rigid eel.



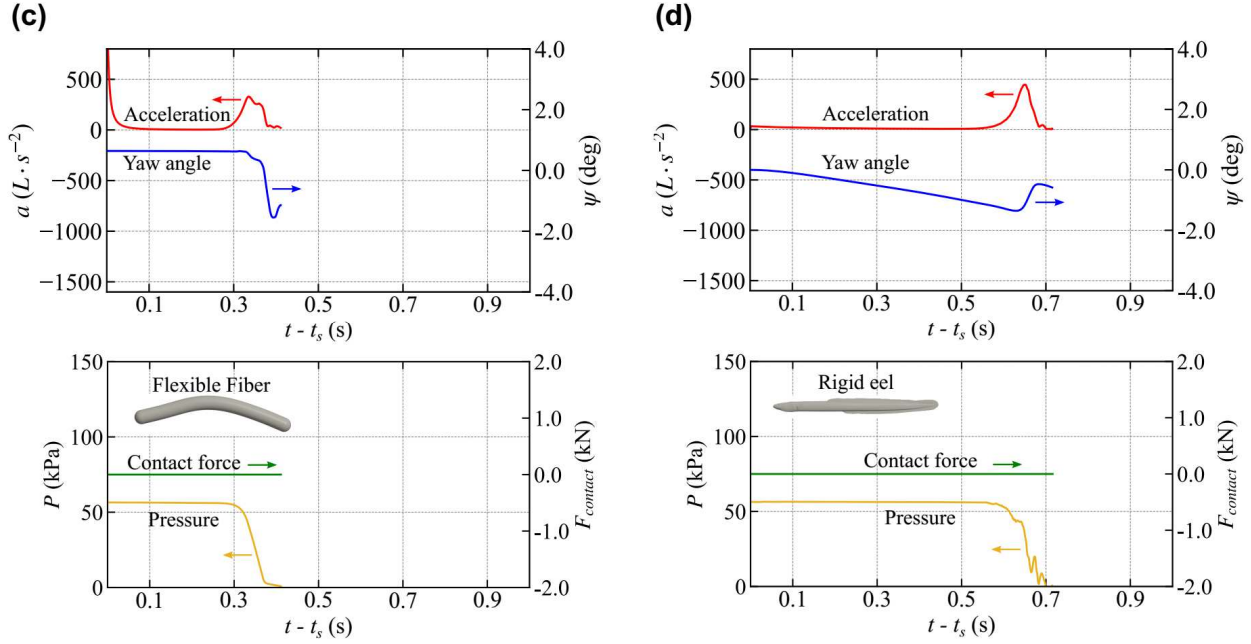


Figure 7. Upper panel: the graph displays acceleration magnitude a (red) and object orientation around Y-axis known as yaw angle ψ (blue) of the object over the time $t - t_s$. Lower panel: the graph displays pressure P (yellow) and contact force magnitude F_{contact} (green) in-between the object and the pipe walls. (a) CFD-DEM super-ellipsoid particle, (b) CFD-DEM composite particle, (c) CFD-DEM flexible fiber, (d) Overset 6-DOF rigid eel.





It must be mentioned that the numerical tracking approaches required additional computations to account for either the motion of interacting discrete objects or the motion of 6-DOF bodies. For comparison purposes, the computational cost of the numerical setup corresponding to each tracking approach was quantified. Table 2 lists the computational costs expressed in CPU time for the suggested tracking approaches and compared to the reference approach when no eel-like object is introduced to the computational domain. For the reference approach, streamlines were used to indicate the trajectory assuming that the object follows the flow streams. The solver was allowed to run for a physical time of almost 8.9 s to obtain a convergent hydrodynamic solution. When CFD-DEM model was activated, the CPU time increased by 11%, 10.6%, and 4.5% for super-ellipsoid particle, composite particles, and flexible fiber, respectively. On the other hand, the overset 6-DOF rigid eel increased the CPU time by a factor of ≈ 6.3 compared to the reference, pure hydrodynamic simulation (no tracked eel-like objects).

Table 2. Computational cost expressed in CPU time for different numerical tracking approaches.

Tracking approach	Streamline (no object)	CFD-DEM super- ellipsoid particle	CFD-DEM composite particle	CFD-DEM flexible fiber	Overset 6-DOF rigid eel
Computational overhead	1 (reference)	1.110	1.106	1.045	6.285

Table 3 presents a qualitative comparison of the different numerical methods used for fish/eel tracking for the above-discussed test case (here, an eccentric reducer). The comparison criteria include accuracy, computational cost, and the capability to model contacts between the object and the wall boundaries.

Table 3. Qualitative comparison between different numerical tracking approaches in terms of accuracy, computational cost, and modeling of the contact in-between traveling objects and walls.

Tracking approach	Streamline (no object)	CFD-DEM super- ellipsoid particle 	CFD-DEM composite particle 	CFD-DEM flexible fiber 	Overset 6-DOF rigid eel 
Accuracy	-	+	++	+++	++++
Computational cost	++++	+	++	+++	-
Contact modeling	-	+	+	+	+

The plus sign (+) indicates advantage, the minus sign (-) indicates disadvantage

4. Discussions

Based on the present findings, it can be said that traditional CFD-DEM methods such as super-ellipsoid particle and composite particles totally failed to accurately predict the eel motion and so the flow-fish interactions in this study. When greater physical realism is required, the boundary-resolved approach using overset 6-DOF rigid eel should be the best choice. However, the overset 6-DOF approach showed more complexity and needs far more computational efforts. The CFD-DEM flexible fiber method gave results close to the one obtained by the overset 6-DOF approach with low computational overhead. It should be noted that all eel-like objects in the current study are modeled as passive objects. Eel behavior, such as escape response and other activities as well as undulatory swimming kinematics, were not considered. Accordingly, future work will seek to implement additional body forces that account for eel activities in our numerical model to mimic more realistically the eel motion. To account for the undulatory swimming in case of flexible fibers, additional deformations can be added under the action of 1) active bending moment due to internal muscular stimulation and 2) passive moment coming from viscoelasticity and damping effects of the eel body. In case of overset 6-DOF eel, the morphing function can be enabled to define an undulatory motion for the rigid eel, corresponding to how eels act in nature.

5. Conclusions

A fish-safe design of hydraulic structures to minimise the risk of fish injury and mortality is necessary for preservation of biodiversity. To achieve this, the development of valuable reliable numerical tools to quantify the sources of injury or mortality to fish and eels during movement is of great importance. Various numerical approaches with varying modelling complexities ranging from flow streamlines to particle-based methods ending with coupled 6-DOF for fish/eel tracking were tested. An eccentric reducer, as a simple closed-conduit component, was considered to demonstrate and compare four numerical methods in terms of accuracy, computational cost, and modeling of the contact in-between traveling objects and walls. It should be noted that the introduced tracking approaches are not limited to pipe flows (the case considered here). They are also applicable for a variety of hydraulic structures including pumps and turbines as well as fishways and bypass facilities. Furthermore, these approaches allow for tracking more than one object traveling through the computational domain for statistical data analyses.

6. ACKNOWLEDGEMENT

The authors wish to thank Jeffrey A. Tuhtan, Assoc. Prof. of Environmental Sensing Technologies at Tallinn University of Technology (TalTech) for providing of the European eel geometry used in this study. This research was funded by the Environment Agency (EA) in UK. The authors declare that this work is a part of a joint PhD carrying out by the first author between Energy and Environment Institute (EEI), University of Hull in UK and Institute of Fluid Dynamics and Thermodynamics (ISUT), Otto von Guericke University Magdeburg in Germany.

7. REFERENCES

Belletti, B., de Leaniz, C.G., Jones, J., Bizzi, S., Börger, L.; Segura, G.,... Barry, J. (2020). "More than one million barriers fragment Europe's rivers." *Nature*, 588, 436–441.

- Boetius, J. (1980). "Atlantic *Anguilla*: a presentation of old and new data of total numbers of vertebrae with special reference to the occurrence of *Anguilla rostrata* in Europe." *Dana*, 1, 1-28.
- Carter, L.J., Thomas, R., Wright, R.M., Collier, S.J., Reeds, J., Murphy L.A. & Bolland, J.D. (2023). "Timing is everything; operational changes at a pumping station with a gravity sluice to provide safe downstream passage for silver European eels and deliver considerable financial savings." *Journal of Environmental Management*, 347, 119143.
- Cox, R.X., Kingsford, R.T., Suthers, I. & Felder, S. (2023) "Fish injury from movements across hydraulic structures: A review." *Water*, 15, 1888.
- Cox, R.X., Lee, O., Perison, W.L., Kammanakada, H., Farzadkhoo, M., Harris, J.H. & Felder, S. (2021) "Preliminary assessment of quantifying fish injury in pipe flow." *Proc., 2nd IAHR Young Professionals Congress*.
- Elena-Maria, K. & Holger, S. (2020) "Mortality assessment for adult European eels (*Anguilla Anguilla*) during turbine passage using CFD modelling." *Renewable Energy*, 147, 1481–1490.
- Garrison, L.A.; Fisher, J.R.K.; Sale, M.J. & Cada, G. (2022) "Application of Biological Design Criteria and Computational Fluid Dynamics to Investigate Fish Survival in Kaplan Turbines." *Proc., HydroVision 2002 Technical Papers*, Portland, OR, USA.
- Huang, Z., Cheng, Y., Wu, J., Diao, W., & Huai, W. (2022). "FSI simulation of dynamics of fish passing through a tubular turbine based on the immersed boundary-lattice Boltzmann coupling scheme." *J. Hydrodyn.*, 34, 135–147.
- Koukouvinis, P. & Anagnostopoulos, J. (2023). "Simulating fish motion through a diagonal reversible turbine." *Energies*, 16, 810.
- Pike, C., Crook, V. & Gollock, M. (2020). "Anguilla anguilla". *The IUCN red list of threatened species 2020*.
- Piper, A.T. & Wright, R.M. (2017). "Understanding fish and eel behaviour to improve protection and passage at river structures." *Environment Agency*, Extended summary - SC120061.
- Powalla, D.; Saha, R.; Hoerner, S. & Thévenin, D. (2022) "Fish injury assessment of a Hydropower facility bypass." *Proc., Conference on modelling fluid flow (CMFF)*, Budapest, Hungary.
- Rezaeiha, A., Montazeri, H., & Blocken, B. (2019) "On the accuracy of turbulence models for CFD simulations of vertical axis wind turbines." *Energy*, 180, 838-857.
- Richmond, M.C., & Romero-Gómez, P. (2014) "Fish passage through hydropower turbines: Simulating blade strike using the discrete element method". *IOP Conf. Series Earth Environ. Sci.*, 22, 062010.
- Richmond, M.C., Serkowski, J.A., Ebner, L.L., Sick, M., Brown, R.S. & Carlson, T.J. (2014) "Quantifying barotrauma risk to juvenile fish during hydro-turbine passage." *Fisheries Research*, 154, 1481–1490.
- Sharma, A., Ananthan, S., Sitaraman, J., Thomas, S., & Sprague, M.A. (2020). "Overset meshes for incompressible flows: On preserving accuracy of underlying discretizations" *J. Comput. Phys.*, 428, 109987.
- Siemens Digital Industries Software. (2023) "Simcenter STAR-CCM+ User Guide", version 2210.0001.
- Watson, J.R., Goodrich, H., Cramp, R.L., Gordos, M.A., & Franklin, C. (2018) "Utilising the boundary layer to help restore the connectivity of fish habitats and populations." *Ecol. Eng.*, 122, 286–294.
- Wright, R.M., Piper A.T., Aarestrup, K., Azevedo, J.M.N., Cowan, G., Don, A.,... Righton D. (2022). "First direct evidence of adult European eels migrating to their breeding place in the Sargasso Sea." *Scientific Reports*, 12, 15362.
- Xue, G., Bai, F., Guo, L., Ren, P. & Liu, Y. (2023) "Research on the effects of complex terrain on the hydrodynamic performance of a deep-sea fishlike exploring and sampling robot moving near the sea bottom." *Front. Mar. Sci.*, 10, 1091523